TECHNISCHE MECHANIK, Band 23, Heft 2-4, (2003), 130– 145
Manuskripteingang: 1. Juli 2003

# Computational Crystal Plasticity : From Single Crystal to Homogenized Polycrystals

G. Cailletaud, O. Diard, F. Feyel, S. Forest

*Jürgen Olschewski zum Gedächtnis*

*Crystal plasticity models for single crystals at large deformation are shown. An extension to the computation of polycrystals is also proposed. The scale transition rule is numerically identified on polycrystal computations, and is valid for any type of loading. All these models are implemented in a finite element code, which has a sequential and a parallel version. Parallel processing makes CPU time reasonable, even for 3D meshes involving a large number of internal variables (more than 1000) at each Gauss point.*

*Together with a presentation of the numerical tools, the paper shows several applications, a study of the crack tip strain fields in single crystals, of zinc coating on a steel substrate, specimen computation involving a large number of grains in each Gauss point. Finally, polycrystalline aggregates are generated, and numerically tested. The effect of grain boundary damage, opening and sliding is investigated.*

## 1 Introduction

Continuum crystal plasticity encompasses a large class of now wide–spread models accounting for the anisotropic deformation of metal single crystals. Its roots are to be found in the works of Taylor, but the complete finite deformation framework is due to the successive contributions of Bilby, Kröner, Teodosiu, Rice and finally Mandel (1973). It is the appropriate framework to simulate the deformation of single crystal specimens under complex loading conditions (tension, shear, torsion, channel die, etc.), but also single crystal components like turbine blades in jet engines (Forest et al. (1996)). Crystal plasticity can be used also to derive the behavior of metal polycrystals from the behavior of individual grains. Such models are now available at two levels. The most predictive version consists in considering sets of interacting grains with a sufficient description of the transgranular behavior (Mika and Dawson (1998); Staroselsky and Anand (1998); Barbe et al. (2001b); Böhlke and Bertram (2001)). This delivers three classes of information : the overall response of the considered material volume that may be close to the wanted effective behavior of the polycrystal, the mean stress and strain for grains having similar crystal orientations, and, finally, the complete heterogeneous stress/strain distribution inside individual grains. The results are obtained through considerable computational effort. That is why simplified homogenization models accounting only for the two first previous information levels are useful. The estimations provided by the Taylor or self–consistent schemes can capture the initial and strain–induced anisotropy of polycrystal behavior from the knowledge of single crystal behavior and material texture described by the orientation distribution function (see references quoted in Cailletaud et al. (2003)). Such models are now very efficient regarding computation time and quality of prediction, so that they can be used for industrial purposes like prediction of texture evolution in metal forming. They can even be included in finite element simulations (Beaudoin et al. (1993); Cailletaud and Pilvin (1994)).

The aim of the present work is to illustrate the panel of computational crystal plasticity models that are now available to describe accurately material behavior ranging from single crystal specimens to polycrystalline metals and alloys. The gain in using such an approach instead of traditional purely phenomenological constitutive theories is emphasized. The computational cost of the use of such methods will be shown to be now attractive enough to compete with more standard design methods. This has to be related to the development of new computational techniques, involving parallel computations, which are specially competitive for this class of models. A short presentation of the used methods will be given. One also includes new advances that push forward the limitations of the classical approach : accounting for size effects, damage and specific grain boundary behavior, etc.

The present work is divided into four main parts. In the first one, the continuum crystal plasticity framework is introduced, starting from a representation of dislocation distribution inside the single crystal volume element. Finite element (FE) computations of stress/strain fields at the crack tip in single crystals are shown as an example. The second one deals with the computation of multicrystalline aggregates. Multicrystals are said here to contain a rather small number of grains, so that the specimen or the component they belong to can be completely meshed with the real grain orientations. The approach is applied to multicrystalline metal coating. The topic of the next part is a discussion of the various scales in an aggregate; a simplified uniform field model involving an explicit scale transition rule is presented. An application in an FE code is shown. The last part concentrates on polycrystalline aggregates, i.e. computational models of a representative volume element (RVE), often artificially generated, to represent bulk polycrystalline metals. Local responses on a granular and intragranular level are analyzed. They demonstrate that grain boundaries play a critical role in the polycrystal behavior. This is the reason why a last type of modeling, including an explicit mesh of the grain boundaries is finally proposed.

## 2 Single Crystal Plasticity

### 2.1 Generalized vs. Classical Crystal Plasticity

Continuum crystal plasticity theory aims at establishing a continuum mechanical framework accounting for the result of complex dislocation glide, multiplication and interaction processes at work in plastically deformed metals. Kröner (1969) proposed to retain the following statistical information out of the intricate entanglement of dislocations contained in a single crystal material volume element :

- the dislocation density tensor $\underset{\sim}{\alpha}$ represents the ensemble average of the tensor product of the dislocation line and Burgers vectors. It is the basic variable of the continuum theory of disclocations and can be directly related to the densities of so–called *geometrically necessary dislocations* $\rho^G$ introduced by Ashby (1971).
- the scalar dislocation density $\rho^S$ denotes the total length of dislocation lines contained in a given volume. It is the basic measure in physical metallurgy and is responsible for a large part of material hardening.

The classical crystal plasticity framework settled by Mandel (1973) and further developed and summarized by Asaro (1983) and Cuitiño and Ortiz (1993), take only the second dislocation density measure into account. It has proved to be a well–suited tool to describe homogeneous and slightly heterogeneous deformation and hardening of single crystals under complex loading conditions. It is based on the definition of crystallographic directors and the introduction of a unique so–called isoclinic intermediate configuration for which the orientation of the directors coincides with the initial one :

$$\underset{\sim}{F} = \underset{\sim}{E}.\underset{\sim}{P}, \quad \dot{\underset{\sim}{P}}.\underset{\sim}{P}^{-1} = \sum_{s=1}^{N} \dot{\gamma}^s \underline{m}^s \otimes \underline{n}^s \tag{1}$$

where the deformation gradient is $\underset{\sim}{F}$, the elastic and plastic deformation tensors are $\underset{\sim}{E}$ and $\underset{\sim}{P}$ respectively. The amount of plastic slip on each slip system $s$ is denoted by $\gamma^s$. The vectors $\underline{m}^s$ and $\underline{n}^s$ represent the slip direction and normal to the slip plane respectively. In the present work, a viscoplastic framework is adopted, together with the classical Schmid law to trigger plastic glide :

$$\dot{\gamma}^s_{cum} = \left\langle \frac{|\tau^s - x^s| - r^s}{k} \right\rangle^n, \quad \dot{\gamma}^s = \dot{\gamma}^s_{cum} \operatorname{sign}(\tau^s - x^s) \tag{2}$$

where $\tau^s, r^s$ and $x^s$ denote the resolved shear stress, the isotropic and kinematic hardening variables, respectively. The isotropic hardening variable is the thermodynamical force associated with an internal variable which usually is more or less directly related to the dislocation densities $\rho^s$. Identifications and applications of such constitutive equations can be found in Méric et al. (1991); Forest et al. (1996) and Cailletaud et al. (2003).

As acknowledged by Mandel (1973) and Sidoroff (1975), the previous classical formulation is a simplified version of a more general model that should incorporate at least the two dislocation density measures introduced at the beginning of this Section. Indeed, such generalized formulations of crystal plasticity have been proposed for instance by Fleck and Hutchinson (1997) and Forest et al. (1997). According to the latter framework, the rotation of the crystal directors is regarded as an actual degree of freedom of the material point independent from its displacement. This leads to the identification of the dislocated crystal with a Cosserat continuum. The kinematics of Cosserat crystal plasticity is illustrated by Fig. 1. The gradient of the lattice rotation tensor is called the lattice

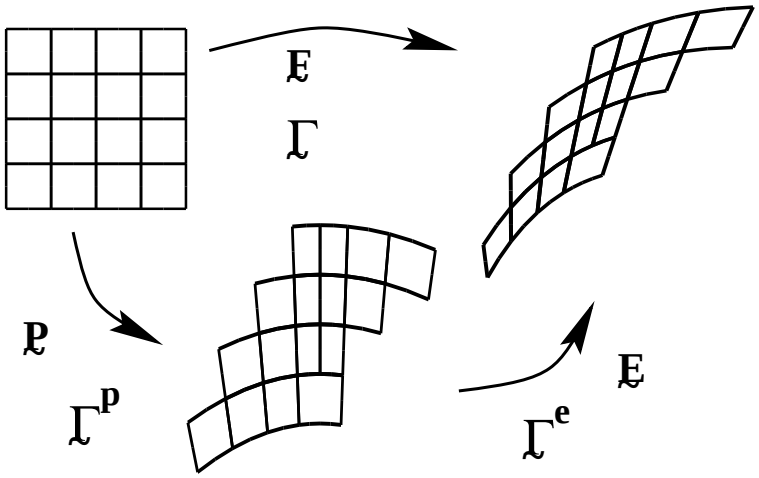


Figure 1: Kinematics of Cosserat single crystal plasticity.

torsion–curvature tensor $\underset{\sim}{\Gamma}$, the plastic part of which directly influences the hardening of the material. This can be seen in the following generalized non–linear isotropic hardening rule

$$r^s = r_0 + Q\sum_{r=1}^{N} h^{sr}(1-\exp(-b\gamma^r_{cum})) + Hl_c\kappa^s \tag{3}$$

The two first terms are the initial critical resolved shear stress and subsequent non–linear hardening including the interaction matrix $h^{rs}$ between the slip systems. The last term is a (for simplicity) linear extra hardening contribution due to the curvature $\kappa^s$ of slip plane $s$ (Forest et al. (2000); Kubin and Mortensen (2003)). The constitutive characteristic length $l_c$ represents the spatial resolution chosen for the continuum crystal plasticity model, below which heterogeneous fields will not be distinguished.

### 2.2 Application to Stress/Strain Fields at a Crack Tip in Single Crystals

When the hardening effect attributed to lattice curvature can be neglected (for large grains under slow strain gradients for example), Fig. 1 reduces to the classical picture of Mandel's multiplicative plasticity. The rotational degrees of freedom reduce to hidden variables. In contrast, lattice curvature effects can play a significant role in the presence of severe strain gradients like those encountered near the crack tip in a single crystal. Fig. 2 shows the plastic strain field at a crack tip in elastic ideally–plastic FCC single crystal under plane strain conditions according to classical crystal plasticity ($H = 0$). The crack plane coincides with the (001) crystal plane and the crack propagation direction is [110]. Three intense deformation bands can be seen intersecting at the crack tip, as expected from Rice's analysis of the problem (Rice (1987)). The crystallographic nature of each band differs depending on its orientation with respect to the crystal. The lateral bands are intense slip bands in which slip lines are parallel to the band. In contrast, the vertical band is called a *kink* band because the slip lines inside are perpenticular to the band (Forest et al. (2001)). Lattice rotation develops only at the boundaries of kink bands, which leads to strong lattice curvature at the band boundaries. The application of Cosserat or strain gradient plasticity can therefore lead to strain fields at the crack tip different from the classical picture. In particular, Fig. 3 shows that parameter $H$ controls the intensity of the vertical kink band in the presented computation. For very high values of the extra hardening parameter, which means a high resistance of the material to lattice curvature, the band can even disappear (Fig. 4). Comparisons between such calculations and experimental results on CT specimens of single crystal nickel base superalloys will be given in a forthcoming publication.

## 3 Computation of Multicrystalline Samples

The previous continuum framework, even if restricted to its classical formulation, has proved to be very efficient and accurate enough to describe stress/strain fields in deformed single crystals under various complex loading conditions (see the references quoted in Cailletaud et al. (2003)). That is the reason why it has been repeatedly used to model material samples containing a finite number of grains that are called here multicrystalline specimens.

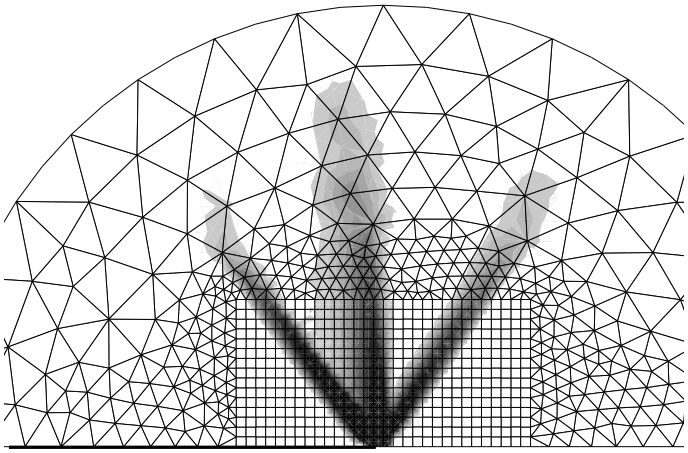

Figure 2: Equivalent plastic strain field at a (001)[110] crack tip according to classical crystal plasticity. The location of the crack is indicated by the bold line.

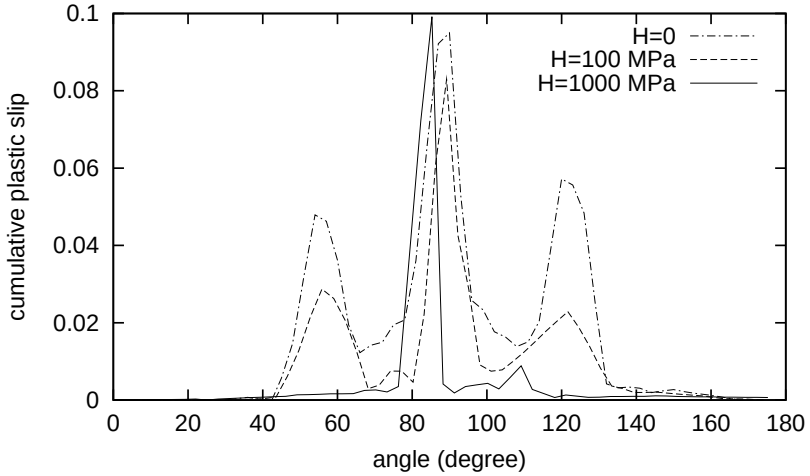


Figure 3: Amount of equivalent plastic slip along a half circle close to the crack tip for three different values of the Cosserat extra–hardening parameter $H$.

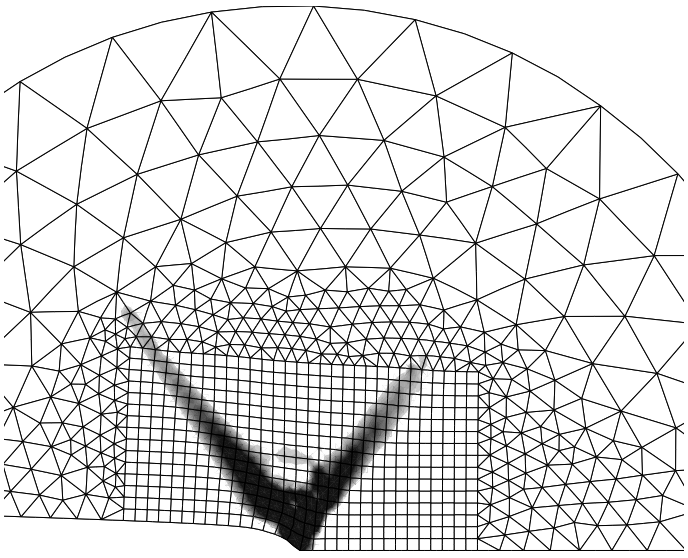

Figure 4: Equivalent plastic strain field at a (001)[110] crack tip according to Cosserat crystal plasticity ($H = 1000$ MPa, deformed geometry showing the crack tip opening).

### 3.1 Coarse Grain Specimens : Simulations vs. Strain/Lattice Rotation Fields Measurements

The strong development of experimental field measurement methods in the last ten years makes it possible to perform accurate comparisons between extensive experimental and numerical results (Ziebs et al. (1996)). The range of validity of continuum crystal plasticity has been tested on recrystallized metal specimens containing a small number of large grains. Electron Back Scatter Diffraction (EBSD) can be used to identify the orientation of all grains. Precise finite element meshes can be designed looking at all sides of the sample, provided that there is no more than 1 or 2 grains within its thickness. Three types of information can be determined experimentally during the deformation of the sample, usually in tension : the lattice rotation field deduced from EBSD analysis at different stages of straining, in–plane strain field using the fiducial micro–grid technique, and elastic strain field based on X–ray analysis. The two first types of measurement were carried out by Delaire et al. (2000) in copper multicrystalline specimens. They reveal the outstanding ability of continuum crystal plasticity to account for the development of non–homogeneous deformation inside grains associated with strain incompatibility between neighbouring grains. Precise lattice rotation measurements are also possible using synchrotron radiation, as done by Eberl et al. (2002) for instance. The intensity of such beams makes it possible to distinguish the lattice rotation induced by straining from the initial mosaicity, i.e. short range fluctuations of crystal orientation, which always exists in large grains. It is not clear up to now which role the initial mosaicity plays on the subsequent deformation of crystals, and whether FE calculations are able to take this into account.

### 3.2 Metal Coatings

Metal coatings are examples of multicrystalline microstructures with high industrial impact. Zinc coatings on galvanized steel sheets for instance are used in the automotive industry. The thickness of the coating studied by Parisot et al. (2001) is 10 $\mu$m, whereas the in–plane grain size is of the order of 300 $\mu$m. This means that the coating contains only one grain within the thickness, and that the microstructure is completely defined by a 2D EBSD map. Zinc has a hexagonal crystallographic structure. The active slip systems are mainly basal and pyramidal $\Pi_2$, as determined by Parisot et al. (2001). Due to the solidification process, the grains have preferred orientations, as the $\underline{c}$–axis of the hexagonal unit cell is close to the vector normal to the steel sheet. Fig. 5(a) shows a finite element map of 34 zinc grains on a steel substrate. For the computations performed for the present work, a recrystallized coating is considered so that the in–plane grain size is reduced to about 30 $\mu$m. The objective of this computation is to analyze the strain gradient that may develop from the interface to the free surface during tensile testing in the plane. The analysis made for the case of pancake grains (300 $\mu$m) revealed that no gradient exists in the thickness except very close to the grain boundaries, as shown by Parisot et al. (2001). The situation becomes very different when the in–plane grain size is closer to the thickness. Fig. 5(b) and (c) give the maps of equivalent plastic strain due to basal slip, which is the mainly activated slip system family. It can be seen that plastic deformation close to the steel/coating interface is significantly more homogeneous than at the free surface. The deformation near the interface is dictated by the quasi–homogeneous deformation of the substrate. In contrast, plastic strain incompatibility from grain to grain induced by different crystal orientations results in strongly heterogeneous plastic slip fields close to the free surface and grain boundaries.

Another important constraining effect due to the substrate has been reported by Parisot et al. (2001). The plastic behavior of zinc single crystals is highly anisotropic. In particular, when the coated sample is strained in direction $x_1$ for instance, the lateral contraction ratio is usually strongly different from $-0.5$ in the zinc grains, depending on its special orientation. For some very specific orientations detailed in Parisot et al. (2001), this ratio is even close to zero. In contrast, the steel substrate behaves almost isotropically. As a consequence, in tension along $x_1$, the substrate prescribes a lateral deformation of about $-\varepsilon_{11}/2$ to the individual grains of the coating. This results in strong biaxial stresses in the zinc grains. That is why pyramidal $\Pi_2$ slip systems and even twinning, which have higher critical resolved shear stresses than basal slip systems, are systematically observed in coatings with pancake grains. Another consequence of this multiaxial stress state inside grains is investigated here. When the lateral expansion ratio is larger than $-1/2$, the lateral stress $\sigma_{22}$ becomes strongly compressive. If a small crack exists or develops at the substrate/coating interface, the finite element computations of Fig. 6 show that a local buckling can occur due to lateral compressive stresses. This is a possible cause for spalling phenomena observed during the stamping of galvanized steel sheets.

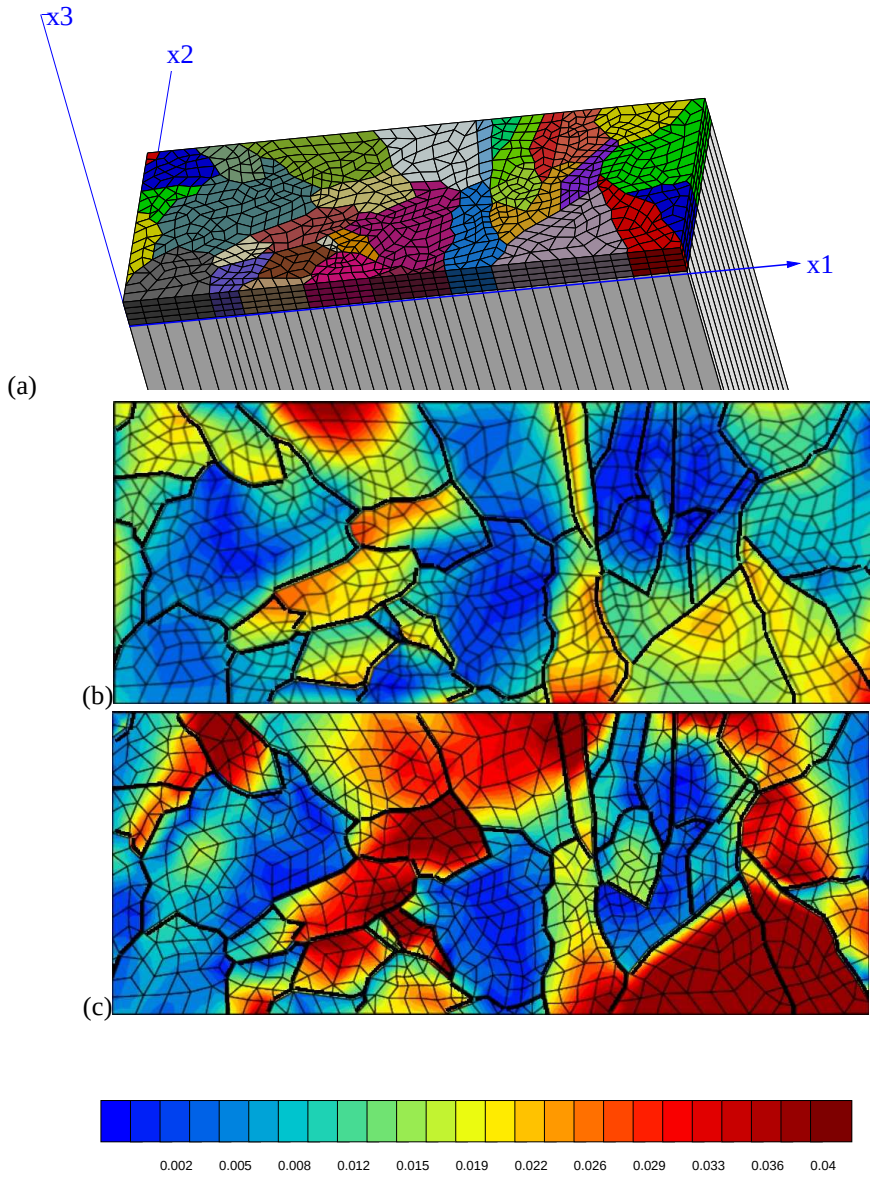


Figure 5: (a) Finite element mesh of 34 grains in a zinc coating on a steel substrate; basal plastic slip distribution (b) in the coating near the interface and (c) on the free surface, for a tensile test in direction $x_1$ up to 1.5 % overall tensile strain (the thick lines coincide with grain boundaries).

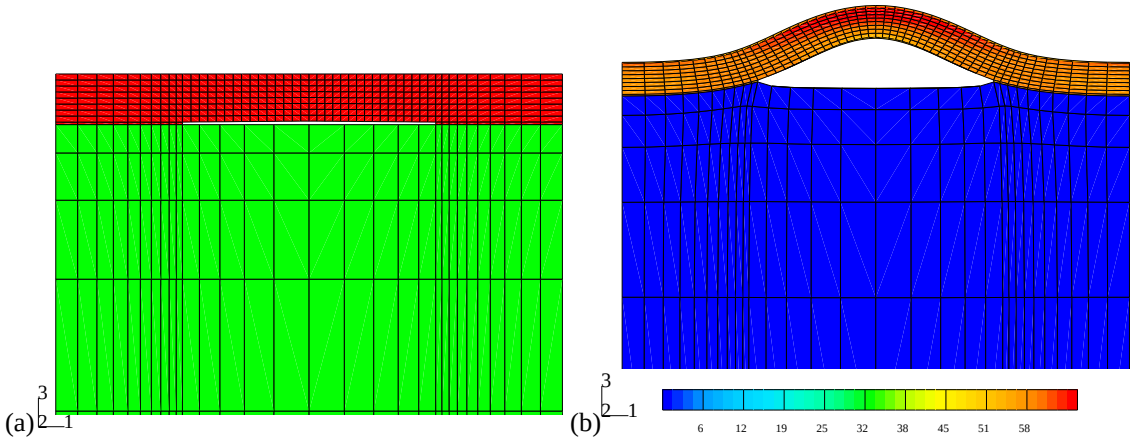


Figure 6: Buckling phenomenon in one grain of a zinc coating on a steel substrate : (a) Finite element mesh showing an initial crack at the substrate/coating interface, (b) plastic slip contour map and deformed state during a tensile test along a direction normal to the figure plane (strain in %).

## 4 Homogenized Polycrystal Models

### 4.1 Levels of Heterogenities and Modeling Strategies in a Polycrystal

Starting from the macroscopic scale (level 1), where a number of grains are considered, several levels can be considered in polycrystal modeling. The mechanical state at each of these levels will be characterized by a stress tensor, a strain tensor, and eventually a series of internal variables. Additional variables can also be introduced to model scale transition.

Let us assume first that each grain has a uniform chemical composition and crystal lattice. Level (2) would correspond to the level of a so–called “phase”. In uniform field models applied to polycrystal modeling, a phase is nothing but the result of the average of all the grains having similar crystal orientations. So stress and strain tensors are the result of an average of all the occurences of this orientation. Note that, since the neighboors of each real grains are different, the averaged quantities in each grain present a certain scatter, related to the local stress redistribution. One could denote the level of each ”real” grain as (2’). Uniform field models will consider phase (2) level, so that a scale transition rule will link macroscopic stress and strain with stresses and strains in each phase.

Level (3) classically corresponds to the local field, which represents intragranular stress and strain variations. These variations are captured only in an FE modeling of the detailed microstructure, and result from the local application of the equilibrium equations. Averaging level (3) variables in a given grain provides a level (2’) response for this grain, and averaging all the (2’) values in the RVE leads to the level (2) variables.

On the other hand, polycrystals can also be multiphase materials (ferrite–austenite, austenite–ferrite–perlite–martensite in steels, for instance). As a rule of thumb, the approximated physical model chosen to represent the microstructure must take into account the strongest heterogenities in the material. Here, the contrast between the properties is larger between austenite to martensite than between two composite grains having a different orientation. Since the main reason for having heterogenities in the RVE is now the nature and the local composition of the material, the most reasonable micro-macro approach will consider an N-phase modeling. A phase will then be defined for each component, disregarding crystal orientation. As a consequence level (2) stress will be defined in austenite, ferrite, etc, and the scale transition rule will start from the macro level to directly reach these phases. Usual criteria like von Mises’s will be used in each phase.

The preceding approach can also be revisited, in order to account for the grain level. The solution is to consider two scale transitions, one from the RVE to the grain level, the grains being represented by their orientation, and the second inside each grain, to get the average stress and strain on each intragranular phase. Depending on the morphology of the phase and the statistical analysis of the distribution, the most efficient transition rule can be the self–consistent, Mori-Tanaka’s, or any other possibility. Such attempts have been made for instance for modeling $\alpha$-$\beta$ Titanium alloys (Feaugas et al. (1996)), or martensitic steels (Cherkaoui et al. (2000)).

### 4.2 Identification of Scale Transition Rules

Homogenized polycrystal models are available to estimate the mean stress–strain in the phases of the polycrystal in the case of elastoplastic, purely viscoplastic and even elastoviscoplastic grain behavior, for instance according to self–consistent schemes (Molinari (1999)). They are usually based on simplified morphological assumptions like that of an inclusion embedded in an infinite matrix combined with a specific pointwise linearization scheme of the non–linear response of the material. A typical form of such a transition law, common to several simplified homogenization schemes, is the following

$$\underset{\sim}{\sigma}^g = \underset{\sim}{\Sigma} + \mu \left( \underset{\sim}{\beta} - \underset{\sim}{\beta}^g \right) \tag{4}$$

$$\underset{\sim}{\beta} = \sum_g f^g \underset{\sim}{\beta}^g, \quad \dot{\underset{\sim}{\beta}}^g = \dot{\underset{\sim}{\varepsilon}}^{pg} - D \dot{\varepsilon}_{eq}^{pg} \underset{\sim}{\beta}^g \tag{5}$$

where non–linear accommodation variables $\underset{\sim}{\beta}^g$ have been introduced by their evolution rules according to Cailletaud (1992) and Pilvin (1996). Elastic isotropy of the grains with shear modulus $\mu$ is assumed for simplicity, and $\dot{\varepsilon}_{eq}^{pg}$ is a norm of the mean plastic strain rate in each phase. The evolution law (5) contains a parameter $D$ which can be calibrated so that the estimated mean stress $\underset{\sim}{\sigma}^g$ is as close as possible to the mean response of the corresponding grains within the polycrystalline aggregate computed via the finite element method. Note that for the value $D = 0$ the model coincides with Kröner's elastoplastic self–consistent scheme. In the case of FCC polycrystals, this single parameter is enough to get a reliable estimation of the behavior of the polycrystal (Cailletaud et al. (2003)).

The formulation of this simplified homogenized polycrystal model, presented here within the small perturbation framework, ends up with the standard crystal plasticity consitutive equations for each crystal orientation subjected to the stress $\underset{\sim}{\sigma}^g$. Finally, the overall increment of plastic deformation is

$$\dot{\underset{\sim}{E}}^p = \sum_g f^g \dot{\underset{\sim}{\varepsilon}}^{pg} \tag{6}$$

where $f^g$ denotes the volume fraction of grains with orientation close to $g$.

This rule can then be extended for more complex cases:
- for time dependent responses, a recovery term can be used in the concentration rule;
- for more anisotropic local responses like for HCP crystals, extensions of the evolution rule (tensorial shape instead of a scalar form) or enhancement of the number of accommodation variables may be necessary;
- for the description of ratchetting effect, a combination of linear and non–linear terms can be introduced in the $\beta$ evolution.

The implementation of such a model in an FE code is not too difficult, since it has the same structure as classical inelastic models. The only difference is the large number of internal variables (with isotropic and kinematic hardening, the number of variables for each phase is twice the number of slip systems). One $\underset{\sim}{\beta}$ tensor is also stored for each phase, that makes $(2N+6) \times G$, with $N$ the number of systems per grain and $G$ the number of grains introduced to represent the texture. The final number is $(2N+6) \times G + 7$ after adding the macroscopic elastic strain and the macroscopic accumulated viscoplastic strain. On the other hand, the integration scheme is the same. For the small perturbation case, the equations set is built from the strain partition equation and the evolution of the internal variables. The local system can be solved by an explicit Runge-Kutta integration, with automatic time step, or with a Newton method, if the number of variables is not too high (typically less than 500). The next section shows an example of such a computation.

### 4.3 Application to Structural Computations

Some elements concerning the computational technique are reported now, then an example is given. A standard finite element code where the unknowns are the incremental nodal displacements contains two major stages :

- *a global stage* : knowing the consistent tangent operator at each integration point, it consists in an assembly to form the stiffness matrix of the problem. An incremental linear problem has to be solved which involves this stiffness matrix. Clearly this stage contains a coupling between all points of the structure; hence it is called a *global stage*. Note also that this global problem is only a *linear* one.

- *a local stage* : the non–linear constitutive equation sets have to be integrated in time to give an estimate of the stress at each integration point (and also to compute the consistent tangent operator). These consitutitive equations (as those presented in section 4.2) are usually non–linear in time. However they remain local in space; this stage may then be seen as a high number of small differential systems to be solved independently.

**The Need for Parallel Computations**

The increasing complexity of mechanical models affects both local and global stages : the global stage becomes more and more complex as soon as the number of degrees of freedom increases to capture fine geometrical aspects of the structures. The local stage is also affected by this increase (because the number of integration points is tied to the number of degrees of freedom), and also by the increasing complexity of constitutive equations.

The local stage is naturally parallel, since the integration of the constitutive equations can be performed independently from the knowledge of the mechanical state of neighboring Gauss points. Attributing groups of elements to a different processor is then a natural and very efficient technique, specially for models with a large number of internal variables. Amdhal's rule recalls that the gain in CPU time for a parallel computation strongly depends on the percentage of parallel operations in the code. It is then necessary to also consider the global stage in the parallel processing.

Domain decomposition methods (DD) are a very good class of methods to overcome these bottlenecks. In this Section we briefly present the FETI method, a specific DD method. The reader may refer to Roux and Farhat (1994) and Feyel (1998) for an extensive description.

Let $\Omega$ be the mesh of the structure and $\Omega_i$ a partition in $N$ subdomains of $\Omega$ : $\Omega = \bigcup_{i=1}^{N} \Omega_i$. Let $\underset{\sim}{B}_i$ be the trace operator which gives the restriction on the boundary of a field defined in $\Omega_i$. The FETI method deals with a condensed interface problem, involving boundary forces on the interfaces. These forces (it is a "dual" method) are estimated using an iterative method that makes the displacement jumps across subdomains vanish. Solving the global linear problem is indeed similar to solving the following subdomains problems simultaneously:

$$\underset{\sim}{K}\vec{q} = \vec{F} \Leftrightarrow \begin{cases} \underset{\sim}{K}_i \vec{q}_i = \vec{F}_i + \vec{\lambda}_i, \text{ local equilibrium of subdomains } \Omega_i \\ \sum_i \underset{\sim}{B}_i \vec{q}_i = \vec{0}, \text{ displacement continuity across subdomains} \end{cases} \tag{7}$$

Depending on the domain decomposition, it can happen that certain local systems are singular. It means that to these subdomains not enough Dirichlet boundary conditions are applied and solid rigid body motions are free. A projected conjugate gradient method is then used involving these rigid body motions, which are determined using the kernel of $\underset{\sim}{K}$. This projection operation is indeed a small problem to be solved on the whole structure considering all domains as solid blocks subjected only to rigid body motions. This provides the extensibility of the method.

An object–oriented finite element code called "ZSet" has been parallelized using this method (Feyel (1998)). A major advantage of DD methods is that they automatically ensure not only the parallelization of the global stage, but also of the local one (a single domain "handles" only the integration points of its domain).

**FE Computation with a Large Number of Internal Variables**

Polycrystal models have been used in the past in FE codes to predict texture evolution. Authors often use Taylor's assumption as a scale transition rule, so that the numerical implementation is straightforward: the global strain rate is just applied to a collection of grains. This assumption is no longer valid for complex and/or cyclic loading paths. In this Section, we show numerical computations using the $\beta$-model, calibrated to model the cyclic hardening of specimens under non proportional 3D loading. Calloch (1997) developed a triaxial specimen, which was tested on the *Astrée* 3D servohydraulic machine in LMT Cachan. This specimen was a central cube undergoing 3D loadings; it allows to study the additional hardening observed in materials like copper or austenitic stainless steels and described by a strain memory effect and indicators measuring the non–proportional character of loading paths in constitutive equations.

Due to the complex shape of the specimen used in 3D experiments and described by Calloch (1997), mechanical fields are not homogeneous, even if the design is such that the central cube undergoes uniform fields: the attaching part of the specimen still plays an important role in the overall behavior. Also, due to the relative dimensions of

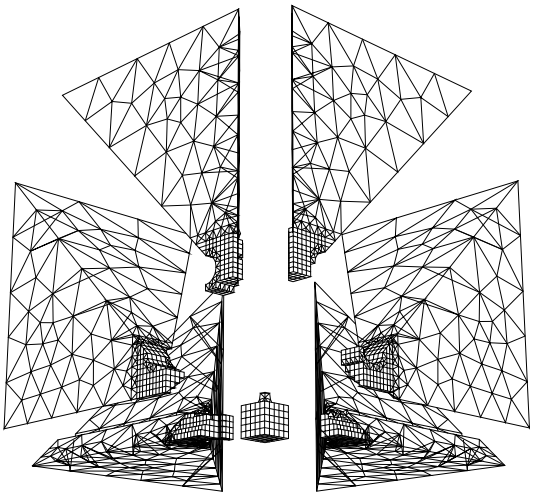

Figure 7: View of the mesh showing the domain decomposition for parallel computing.

the cube with respect to the specimen, neither strain gauges nor extensometers can be used to get the real loading conditions prescribed to the central part. FE computations are then needed to analyze the test results.

The polycristalline model is a good candidate for these computations. A detailed description of the results can be found in Feyel et al. (1997). Seven years ago, CPU time was about one week. With a simple PC cluster, the same computations would now take less than one day for several loading cycles. One $8^{th}$ of the specimen is modeled. The mesh contains 8288 quadratic elements, 3358 nodes and 69090 integration points. A domain decomposition into seven subdomains is performed (see Fig. 7). The normal displacement of the side faces are fixed in order to respect the symmetry of the problem. A cyclic loading is applied on the external faces. The polycrystalline constitutive equation set contains 40 grains; 1207 internal variables are then necessary at each integration point of the mesh, that is about 83 millions for the whole mesh. A great advantage of such a modeling is to allow a simultaneous two scale analysis, on a macro and a micro scale. Fig. 8 shows the contour plots of $\sigma_{11}$ at the end of the computation.

A microscopic analysis is also available by carefully post-processing the instantaneous and cumulated slip for each system and each grain. For instance, Fig. 9 shows the evolution of the number of active slip systems, at three different times during the computation. These values are computed at the center of the specimen. A slip system is said to be active when the slip rate is higher than a predefined threshold. At the beginning of the loading, a certain number of slip systems are active for all grains. This number increases with accumulated plastic strain.

## 5 Computation of Polycrystalline Aggregates

Polycrystalline aggregates are computational models for a representative volume element (RVE), often artificially generated, to represent polycrystalline materials. They can be used to calibrate the transition rule of the model shown in Section 4.2 (level (2)), and also to evaluate level (3) fields, in order to investigate local effects due to the free surface or to grain boundaries.

### 5.1 Typical Results

A method for generating polycrystalline aggregates has been shown in Barbe et al. (2001a). It uses a Voronoi tesselation of a given volume, the initial germs being installed by simulating a Poisson point process. The result is a voxel file, defining grain orientation in each point inside the RVE. The next step is a mesh generation which respects the microstructure. Two solutions can be found in the literature, a regular mesh involving multimaterial elements (Fig. 10a) and meshes respecting the shape of the grain (Fig. 10b). The first solution is simpler and can provide good results, even if the number of elements is relatively low. In fact, the result depends on the contrast between the different phases. For instance for FCC aggregates, the global response becomes constant for cubic meshes involving more than $14 \times 14 \times 14$ elements and 200 crystal orientations. The same order of magnitude

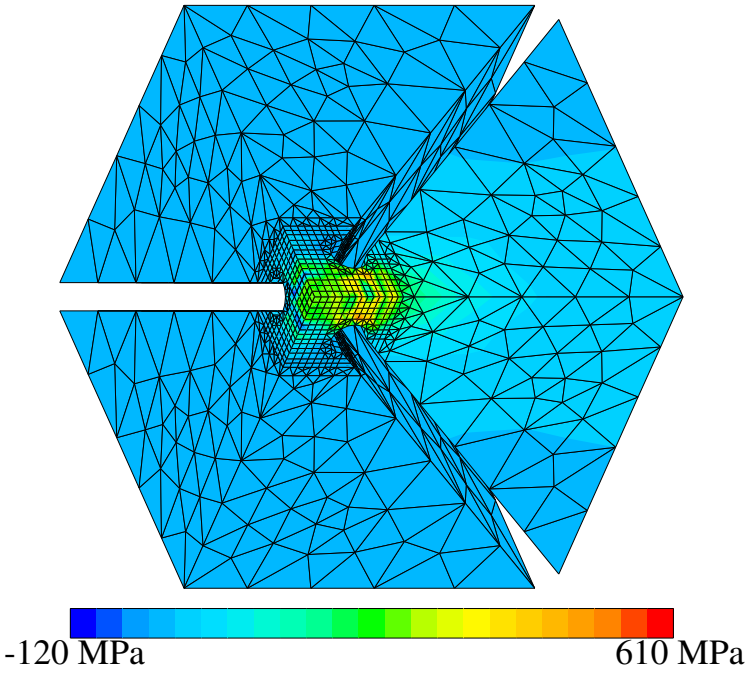


Figure 8: Contour of the $\sigma_{11}$ stress component at the end of the computation.

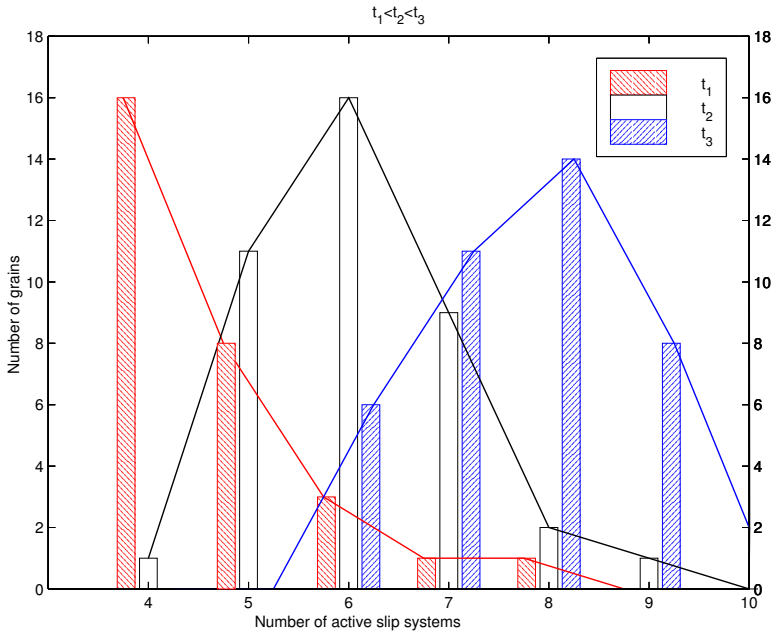


Figure 9: Distribution of the number of active slip systems for the central point of the specimen.

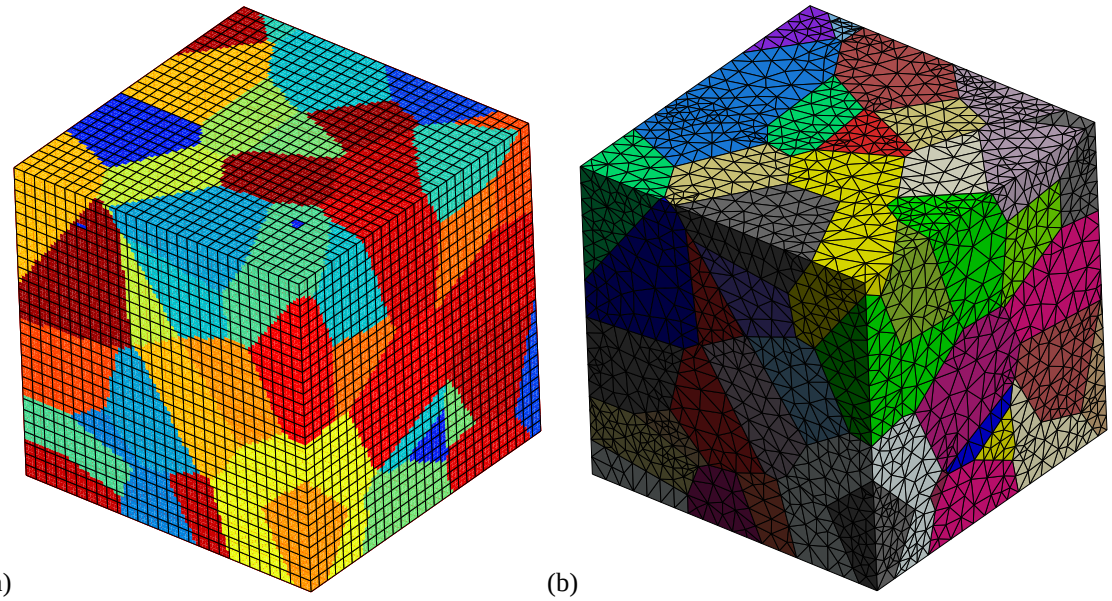

(a) (b)

Figure 10: Two meshing strategies for the polycrystalline aggregate : (a) regular mesh, (b) mesh respecting the grain boundaries.

is observed for HCP alloys (see Diard et al.). Nevertheless, if the scatter in the local properties is high, the real convergence is not reached even for very large meshes. On the other hand, multimaterial elements do not allow to give a realistic view on the grain boundaries. Their use should then be limited to investigations of the global response, or to qualitative response in the grains, except if a very large number of elements is used (more than $30 \times 30 \times 30$ elements, several thousands of Gauss points per grain). They are also not adapted for the description of intergranular damage.

Fig. 11 shows a typical result concerning the local fields of the total strain in the tensile direction and the von Mises stress. The material is a Zy4 alloy, identified in Diard et al.. The coefficients have been determined from tension and internal pressure tests on tubes. The von Mises stress is higher at the grain boundaries. On the other hand, the deformation is localized in bands which do not follow the grain boundaries. The present calculations are made with a $28 \times 28 \times 28$ mesh with 20-node quadratic elements and full integration. The integration point size can be seen on the picture. In order to improve the description, developments have been made to explicitely account for grain boundaries. The used model is presented in the next Section, and new results with the same material are shown at the end of the paper.

### 5.2 The DOS Model for Grain Boundary Damage, Opening and Sliding

The behavior of a grain boundary is highly anisotropic. It must be defined in a local frame, built from the local normal $\underline{n}$ to the grain boundary and two tangent vectors in the grain boundary. The normal direction is quite strong as long as no damage is present, but the in-plane elastic moduli are weak. As a consequence, the only significant terms in the stress and strain tensors are:
- the normal stress $\sigma^n$ and the normal strain $\varepsilon^n$, which define grain boundary opening;
- the shear stress $\tau$ and the shear strain $\varepsilon^t$, which define grain boundary sliding.

The problem of the grain boundary opening and sliding is similar to interface debonding. This last problem has been studied in the past (Needleman (1990); Chaboche et al. (2001)), by introducing special elements. The present approach will use a regular continuous element, that makes it easier to manage damage.

In the chosen framework, the grain boundary can first have a viscoplastic motion when the loading starts. Damage will then develop, and enhance opening and sliding. The damage evolution rule is written in terms of $Y$, which is its conjugated variable, according to classical damage mechanics (Lemaitre and Chaboche (1990)), and uses $E$, the elastic modulus in the normal direction, and $\mu$, the shear modulus in the plane of the grain boundary:

$$Y = \frac{\sigma^{n2}}{E} + \frac{\tau^2}{\mu} \tag{8}$$

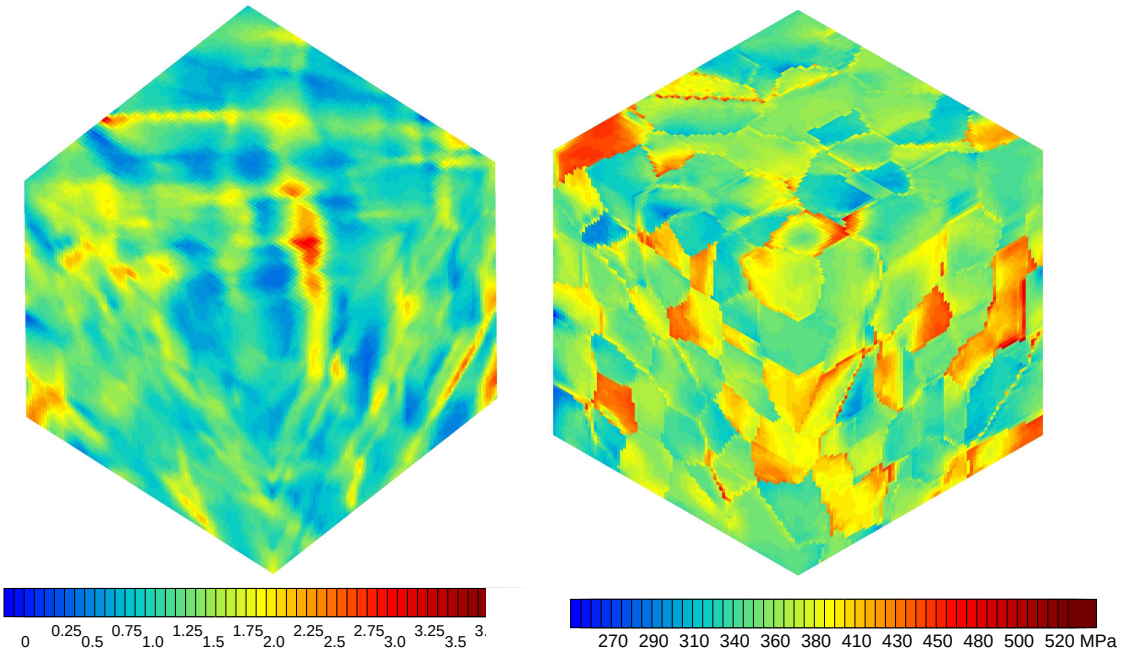


Figure 11: Contour (a) of the total strain in the tensile direction, (b) of von Mises equivalent stress, for the aggregate shown in Fig. 10.

The basic equations are defined according to the following scheme.

| Effect | Potential | with... |
|---|---|---|
| normal strain | $F_n = K_n \left\langle \frac{f^n}{K_n} \right\rangle^{n_n+1}$ | $f_n = < \sigma^n > /(1-D) - R_n$ |
| shear strain | $F_t = K_t \left\langle \frac{f^t}{K_t} \right\rangle^{n_t+1}$ | $f_t = \lvert\tau\rvert/(1-D) - R_t$ |
| damage | $F_D = K_D \left\langle \frac{f^D}{K_D} \right\rangle^{n_D+1}$ | $f_D = \sqrt{\frac{Y}{E(1-D)}} - R_D$ |

Three independent potentials are defined from three threshold functions involving damage, normal stress and shear stress. These potentials naturally provide a flow rate and a damage rate. One can see that shear and opening strain are not coupled at the onset of plastic flow. Nevertheless, damage development will produce coupling between them: as shown in equation 9, if the normal (resp. tangential) stress produces damage, it will increase the tangential (resp. the normal) strain rate.

$$\dot{\underset{\sim}{\varepsilon}}^n = \frac{\partial F_n}{\partial \underset{\sim}{\sigma}} = \frac{\partial F_n}{\partial f_n}\frac{\partial f_n}{\partial \underset{\sim}{\sigma}} = \left\langle \frac{< \sigma^n > /(1-D) - R_n}{K_n} \right\rangle^{n_n} \underline{n} \otimes \underline{n} = \dot{\delta} \underset{\sim}{N}$$

$$\dot{\underset{\sim}{\varepsilon}}^t = \frac{\partial F_t}{\partial \underset{\sim}{\sigma}} = \frac{\partial F_t}{\partial f_t}\frac{\partial f_t}{\partial \underset{\sim}{\sigma}} = \left\langle \frac{\lvert\tau\rvert/(1-D) - R_t}{K_t} \right\rangle^{n_t} \{\underline{n} \otimes \underline{t}\} = \dot{\gamma} \underset{\sim}{T}$$

$$\dot{D} = \frac{\partial F_D}{\partial Y} = \frac{\partial F_D}{\partial f_D}\frac{\partial f_D}{\partial Y} = \left\langle \sqrt{\frac{Y}{E}} \frac{1}{1-D} - R_D \right\rangle^{n_D} \frac{1}{\sqrt{EY(1-D)}}$$

### 5.3 Explicit Grain Boundary Meshing

Typical results obtained with the DOS model are illustrated in Fig. 12 on a 2D mesh. As shown in Fig. 12a, the development of intergranular damage will produce a softening of the material. The damage field is shown in Fig. 12c, for a vertical tensile loading. Since there is no specific surface effect in the computation, damage

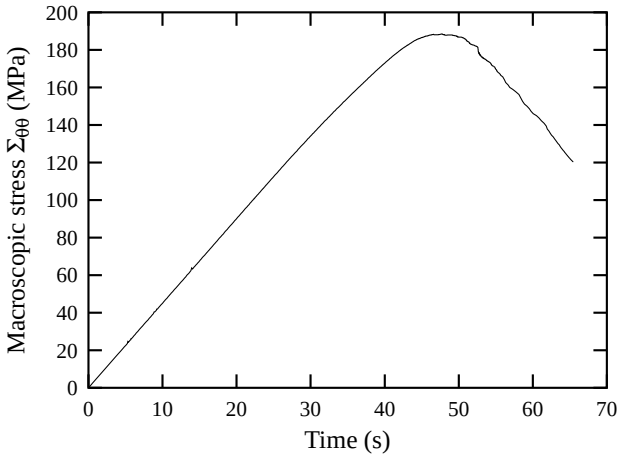


(a)

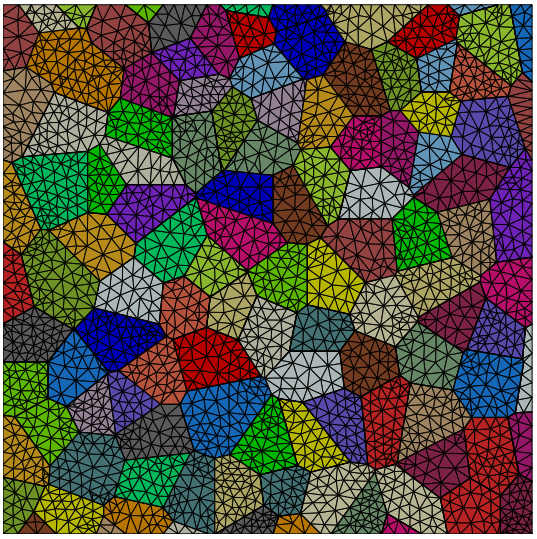

(b)

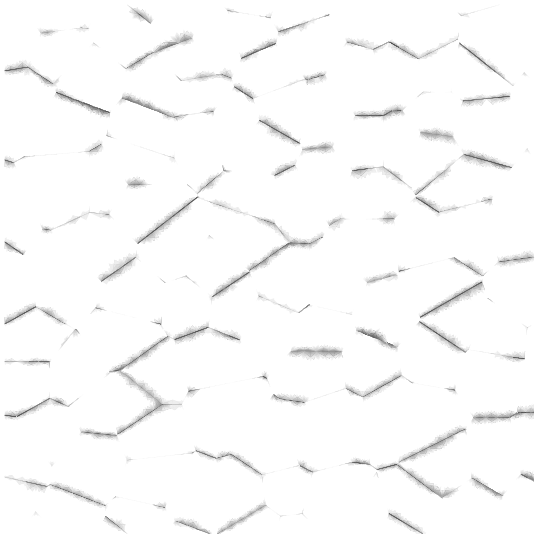

(c)

Figure 12: Illustration of 2D computations with grains and grain boundaries with DOS model: (a) the global load response, (b) the mesh, (c) resulting intergranular damage field.

develops anywhere in the material, the grain boundaries perpendicular to the external loading being preferentially affected. The damage path can be checked using the second plot (Fig. 12b), in which the grain boundary elements are present between grains.

## 6 Conclusion and Future Work

Crystal plasticity is now the engine of a lot of models. It has already been applied in FE codes by a series of researchers and engineers. From an industrial point of view, the most significant computations have been performed to predict texture evolutions, with relatively crude scale transition rules. The present paper shows that structural computations (here on a specimen) can be made also with more realistic models, valid also under cyclic loadings. On the other hand, the first computations in the literature have been made on 2D meshes. The more recent approaches of the problem tend to introduce real or realistic microstructures, and to replace 2D meshes, which only capture qualitative responses, by 3D meshes, in order to provide quantitative results. It means that the numerical models are now able to switch from the global to the local level, with a reasonable CPU time, provided parallel processing is introduced into the code.

Crystal plasticity in a parallel FE code represents a powerful computational tool to investigate the local stress and strain in heterogeneous materials. It allows also to solve problems in which global and local scales are not well separated. The computation of microstructures will then be used in the future to better understand the local deformation and failure mechanisms. The present paper shows examples concerning crack tip in single crystals, zinc coating layers on steels, and deformation of HCP polycrystalline aggregates.

Starting at a millimetric size, the crystal plasticity approach tends to lower scales. The purpose is then to bridge the gap between the macroscale and "less than micrometric" scales, where dislocation densities, and other methods originating from physics are developed. New models and new techniques are to be developed to allow fruitful discussion between scientists from both sides. Generalized formulations of plasticity theory to account for high gradients which are predicted by the computations, and also more sophisticated mesh generation tools, coupled with error control, represent the challenge to come in the near future.

**References**


Asaro, R.: Crystal plasticity. *J. Appl. Mech.*, 50, (1983), 921–934.

Ashby, M.: The deformation of plastically non-homogeneous alloys. In: A. Kelly; R. Nicholson, eds., *Strengthening Methods in Crystals*, pages 137–192, Applied Science Publishers, London (1971).

Barbe, F.; Decker, L.; Jeulin, D.; Cailletaud, G.: Intergranular and intragranular behavior of polycrystalline aggregates. Part I: FE model. *Int. J. of Plasticity*, 17, 4, (2001a), 513–536.

Barbe, F.; Forest, S.; Cailletaud, G.: Intergranular and intragranular behavior of polycrystalline aggregates. part 2: Results. *International Journal of Plasticity*, 17, (2001b), 537–563.

Beaudoin, A.; Mathur, K.; Dawson, P.; Johnson, G.: Three–dimensional deformation process simulation with explicit use of polycrystal plasticity models. *International Journal of Plasticity*, 9, (1993), 833–860.

Böhlke, T.; Bertram, A.: The evolution of Hooke's law due to texture development in polycrystals. *Int. J. Solids Struct.*, 38, (2001), 9437–9459.

Cailletaud, G.: A micromechanical approach to inelastic behaviour of metals. *Int. J. of Plasticity*, 8, (1992), 55–73.

Cailletaud, G.; Forest, S.; Jeulin, D.; Feyel, F.; Galliet, I.; Mounoury, V.; Quilici, S.: Some elements of microstructural mechanics. *Computational Materials Science*, 27, (2003), 351–374.

Cailletaud, G.; Pilvin, P.: Utilisation de modèles polycristallins pour le calcul par éléments finis. *Revue Européenne des Éléments Finis*, 3, 4, (1994), 515–541.

Calloch, S.: *Essais triaxiaux non-proportionnels et ingénierie des modèles de plasticité cyclique*. Ph.D. thesis, École Normale Supérieure de Cachan (1997).

Chaboche, J. L.; Feyel, F.; Monerie, Y.: Interface debonding models: a viscous regularization with a limited rate dependency. *Int. J. Solids Structures*, 38, (2001), 3127–3160.

Cherkaoui, M.; Berveiller, M.; Lemoine, X.: Couplings between plasticity and martensitic phase transformation: overall behavior of polycrystalline trip steels. *Int. J. of Plasticity*, 16, (2000), 1215–1241.

Cuitiño, A.; Ortiz, M.: Computational modelling of single crystals. *Modelling Simul. Mater. Sci. Eng.*, 1, (1993), 225–263.

Delaire, F.; Raphanel, J.; Rey, C.: Plastic heterogeneities of a copper multicrystal deformed in uniaxial tension: experimental study and finite element simulations. *Acta mater.*, 48, (2000), 1075–1087.

Diard, O.; Leclercq, S.; Rousselier, G.; Cailletaud, G.: Evaluation of finite element based analysis of 3d multicrystalline aggregates plasticity. *submitted*.

Eberl, F.; Forest, S.; Wroblewski, T.; Cailletaud, G.; Lebrun, J.-L.: Finite element calculations of the lattice rotation field of a tensile loaded nickel base alloy multicrystal and comparison to topographical X-ray diffraction measurements. *Metallurgical and Materials Transactions*, 33A, (2002), 2825–2833.

Feaugas, X.; Pilvin, P.; Clavel, M.: Cyclic deformation behaviour of an alpha/beta titanium alloy : II. internal stresses and micromechanic modelling. *Acta Metall.*.

Feyel, F.: *Application du calcul parallèle aux modèles à grand nombre de variables internes*. Ph.D. thesis, École Nationale Supérieure des Mines de Paris (1998).

Feyel, F.; Calloch, S.; Marquis, D.; Cailletaud, G.: F.e. computation of a triaxial specimen using a polycrystalline model. *Comp. Material. Sci.*, 9, (1997), 141–157.

Fleck, N.; Hutchinson, J.: Strain gradient plasticity. *Adv. Appl. Mech.*, 33, (1997), 295–361.

Forest, S.; Barbe, F.; Cailletaud, G.: Cosserat modelling of size effects in the mechanical behaviour of polycrystals and multiphase materials. *International Journal of Solids and Structures*, 37, (2000), 7105–7126.

Forest, S.; Boubidi, P.; Sievert, R.: Strain localization patterns at a crack tip in generalized single crystal plasticity. *Scripta Materialia*, 44, (2001), 953–958.

Forest, S.; Cailletaud, G.; Sievert, R.: A Cosserat theory for elastoviscoplastic single crystals at finite deformation. *Archives of Mechanics*, 49, 4, (1997), 705–736.

Forest, S.; Han, J.; Pilvin, P.; Olschewski, J.: Parameter identification for anisotropic gas turbine blade alloys. In: J. Désidéri; C. Hirsch; P. L. Tallec, eds., *ECCOMAS Computational methods in applied sciences'96*, pages 393–400, J. Wiley (1996).

Kröner, E.: Initial studies of a plasticity theory based upon statistical mechanics. In: K. M.F.; A. W.F.; R. A.R.; J. R.I., eds., *Inelastic Behaviour of Solids*, pages 137–147, McGraw-Hill, New York (1969).

Kubin, L.; Mortensen, A.: Geometrically necessary dislocations and strain–gradient plasticity. *Scripta materialia*, 48, (2003), 119–125.

Lemaitre, J.; Chaboche, J.-L.: *Mechanics of Solid Materials*. Cambridge University Press, Cambridge, U.K. (1990).

Mandel, J.: Equations constitutives et directeurs dans les milieux plastiques et viscoplastiques. *Int. J. Solids Structures*, 9, (1973), 725–740.

Méric, L.; Poubanne, P.; Cailletaud, G.: Single crystal modeling for structural calculations. Part 1: Model presentation. *J. Engng. Mat. Technol.*, 113, (1991), 162–170.

Mika, D.; Dawson, P.: Effects of grain interaction on deformation in polycrystals. *Material Science Engineering*, A257, (1998), 62–76.

Molinari, A.: Extensions of the self-consistent tangent model. *Modelling Simul. Mater. Sci. Eng.*, 7, (1999), 683–697.

Needleman, A.: Analysis of tensile decohesion along an interface. *J. Mech. Phys. Sol.*, 38, (1990), 289–324.

Parisot, R.; Forest, S.; Gourgues, A.-F.; Pineau, A.; Mareuse, D.: Modeling the mechanical behavior of a multicrystalline zinc coating on a hot-dip galvanized steel sheet. *Computational Materials Science*, 19, (2001), 189–204.

Pilvin, P.: The contribution of micromechanical approaches to the modelling of inelastic behaviour of polycrystals. In: A. Pineau; G. Cailletaud; T. Lindley, eds., *Fourth Int. Conf. on Biaxial/multiaxial Fatigue and Design*, pages 3–19, ESIS 21, Mechanical Engineering Publications, London (1996).

Rice, J.: Tensile crack tip fields in elastic-ideally plastic crystals. *Mechanics of Materials*, 6, (1987), 317–335.

Roux, F. X.; Farhat, C.: Implicit parallel processing in structural mechanics. *Comp. Meth. Appl. Mecha. Eng.*, 2, 1.

Sidoroff, F.: Microstructure and plasticity. *Mech. Res. Comm.*, 2, (1975), 73–77.

Staroselsky, A.; Anand, L.: Inelastic deformation of polycrystalline f.c.c. materials by slip and twinning. *J. Mech. Phys. solids*, 46, (1998), 671–696.

Ziebs, J.; Bressers, J.; Frenz, H.; Hayhurst, D.; Klingelhöffer, H.; Forest, S.: *Proceedings of the International Symposium on Local strain and temperature measurements in non-uniform fields at elevated temperatures, Berlin*. Woodhead Publishing Limited (1996).

---

*Address:* Prof. Georges Cailletaud and Dr. Samuel Forest, Centre des Matériaux/UMR 7633, Ecole des Mines de Paris/CNRS, BP 87, F-91540, Evry, email: georges.cailletaud@ensmp.fr,samuel.forest@ensmp.fr, Dr. Olivier Diard, Electricité de France, Division R&D, F-77818 Moret s/ Loing, email: olivier.diard@edf.fr, Dr. Frédéric Feyel, ONERA/DMSE/LCME, 29 avenue de la Division Leclerc, BP 72, F-92322 Châtillon, email: feyel@onera.fr